Combined ^{18}F-FDG and ^{11}C-Methionine PET Scans in Patients with Newly Progressive Metastatic Prostate Cancer

Rodolfo Nuñez, MD[1]; Homer A. Macapinlac, MD[1]; Henry W.D. Yeung, MD[1]; Tim Akhurst, MD[1]; Shangde Cai, PhD[2]; Iman Osman, MD[3]; Mithat Gonen, PhD[4]; Elyn Riedel, MA[4]; Howard I. Scher, MD[3]; and Steven M. Larson, MD[1]

[1]Nuclear Medicine Service, Department of Radiology, Memorial Sloan-Kettering Cancer Center, New York, New York; [2]Cyclotron Core Facility, Sloan-Kettering Institute and Memorial Sloan-Kettering Cancer Center, New York, New York; [3]Genitourinay Oncology Service, Department of Medicine, Memorial Sloan-Kettering Cancer Center, New York, New York; and [4]Department of Epidemiology and Biostatistics, Memorial Sloan-Kettering Cancer Center, New York, New York

Metastatic prostate cancer may respond initially to hormone suppression, with involution of tumor sites, but ultimate tumor progression is inevitable. Our aim was to detect the proportion of bone and soft-tissue lesions that represent metabolically active tumor sites in patients with progressive metastatic prostate cancer. **Methods:** In a prospective study, we compared ^{18}F-FDG and L-*methyl*-^{11}C-methionine (^{11}C-methionine) PET with conventional imaging modalities (CIM), which included the combination of ^{99m}Tc-methylene diphosphonate scintigraphy, CT, or MRI. Twelve patients with prostate cancer, increasing levels of prostate-specific antigen (PSA), and at least 1 site (index lesion) with new or increasing disease on CIM were studied. The total numbers of soft-tissue and bone-tissue lesions, in a site-by-site comparison, were calculated for all imaging modalities. **Results:** The sensitivities of ^{18}F-FDG PET and ^{11}C-methionine PET were 48% (167/348 lesions) and 72.1% (251/348 lesions), respectively, with CIM being used as the 100% reference (348/348). ^{11}C-Methionine PET identified significantly more lesions than ^{18}F-FDG PET ($P < 0.01$). All 12 patients with progressive metastatic prostate cancer had at least 1 lesion site of active metabolism for ^{18}F-FDG or ^{11}C-methionine, which could be used as an index lesion to monitor the metabolic response to therapy. A significant proportion of lesions (26%) had no detectable metabolism of ^{18}F-FDG or ^{11}C-methionine. Although technical factors cannot be totally excluded, we believe that metabolically inactive sites may be necrotic or dormant. More than 95% (251/258) of metabolically active sites (72% of the total number of lesions detected by CIM) metabolize ^{11}C-methionine. ^{18}F-FDG uptake is more variable, with 65% of metabolically active sites (48% of the total number of lesions detected by CIM). **Conclusion:** These findings reflect the different biologic characteristics of the lesions in a heterogeneous tumor such as prostate cancer and suggest that a time-dependent metabolic cascade may occur in advanced prostate cancer, with initial uptake of ^{11}C-methionine in dormant sites followed by increased uptake of ^{18}F-FDG during progression of disease.

Received Feb. 20, 2001; revision accepted Sep. 25, 2001.

For correspondence or reprints contact: Rodolfo Nuñez, MD, Division of Nuclear Medicine, Long Island Jewish Medical Center, 270-05 76th Ave., New Hyde Park, NY 11040.

E-mail: rnunez@lij.edu

Key Words: PET; ^{18}F-FDG; ^{11}C-methionine; bone scan; prostate cancer

J Nucl Med 2002; 43:46–55

Prostate carcinoma represents the most common malignancy in men in the United States. An estimated 184,500 men were affected in 1998, with fatal outcomes in 39,200 cases, making this the second leading cancer killer in men behind lung cancer (*1*). As a result of vascular spread, approximately 30% of these patients show bony metastasis at the time of diagnosis and >80% show bony metastasis at the time of death (*2*,*3*). Through lymphatic spread the metastasis can involve, in decreasing order, the obturator, internal iliac, common iliac, presacral, and paraaortic nodes. Hematogenous metastasis occurs in bone much more frequently than in lung, liver, and adrenal glands (*4*).

Radical prostatectomy and radiotherapy represent the 2 main curative modalities in cases of localized disease; however, hormonal manipulation is generally accepted as the treatment of choice in metastatic disease. Still, there is much controversy in some aspects of patient management. One of several reasons for these controversies is that the malignancy is heterogeneous, ranging from a relatively indolent tumor in some patients to an extremely aggressive disease in other patients.

Recent developments of high-resolution imaging modalities, such as MRI and spiral CT, have contributed to the early detection and more accurate staging of malignant tumors because of precise morphologic information on the lesion and surrounding normal tissue. However, these imaging modalities and bone scintigraphy are limited in their ability to distinguish benign from malignant masses, such as determining if a slightly enlarged lymph node is involved by cancer. Thus, an obvious need exists for better imaging modalities that could more accurately characterize individual lesions in vivo so that decisions regarding treatment

options in a particular patient could also be based on knowledge of the metabolic activity and biologic characteristics of the tumor. Furthermore, better assessment of response to therapy is also of great importance.

PET with ^{18}F-FDG, a tracer of glucose metabolism, has been highly successful for imaging a wide variety of tumors and for monitoring response to therapy (*5*). This agent is transported, phosphorylated, and metabolically trapped into tumor cells as a glucose substitute (*6*).

L-*methyl*-^{11}C-Methionine (^{11}C-methionine) is also used to image a variety of tumors, including lymphomas and tumors of the brain, lung, and head or neck. ^{11}C-Methionine accumulation in tumor cells is attributed to increased amino acid transport and metabolism (*7,8*). However, only a few clinical studies have compared ^{18}F-FDG PET and ^{11}C-methionine PET in detecting tumor lesions in the same patient, and none of these studies was with prostate cancer patients (*9–11*).

This study's aim was to assess the strengths and limitations of imaging patients with progressive metastatic prostate cancer with ^{18}F-FDG PET and ^{11}C-methionine PET, in comparison with conventional imaging modalities (CIM), which included the combination of bone scanning, CT, and MRI.

MATERIALS AND METHODS

Patients were recruited prospectively and entered into the PET protocol study after written informed consent was obtained, following the Institutional Review Board Guidelines of our institution. From this group of patients, we included in our study the first 12 who had whole-body ^{18}F-FDG PET and ^{11}C-methionine PET on the same day.

Patient Eligibility Criteria

Patients had histologically proven prostate adenocarcinoma and disease progression as shown by (a) a >50% increase in serum prostate-specific antigen (PSA) levels sustained for a minimum of 3 observations obtained at least 1 wk apart, and (b) development of new lesions or worsening of preexisting lesions on bone scintigraphy, CT, or MRI.

Pretreatment Evaluation

Patient evaluation included history and physical examination, complete blood count, PSA (within 2 wk of study entry), and urinalysis to exclude urinary tract infection (within 2 wk). Bone scintigraphy, modified MRI of the pelvis to image the prostate (including the retroperitoneum), CT of the abdomen and pelvis, and chest radiography (all of them done within 4 wk of the PET scan) were also included.

^{11}C-Methionine PET

The cyclotron core facility staff of our institution provided the radiopharmaceuticals. ^{11}C-Methionine was synthesized using a modification of the method described by Ishiwata et al. (*7*).

All patient scanning was performed on an Advance PET scanner (General Electric Medical Systems, Milwaukee, WI). This camera has a field of view of 55 cm in diameter and 15.2 cm in axial length. All scanning was performed in 2-dimensional (septa in) mode. The transaxial resolution is 3.8 mm full width at half maximum (FWHM) at the center of the field of view, increasing to 7.3 mm at a radial distance of 20 cm. The average axial resolution decreases from 4.0 mm FWHM at the center to 6.6 mm at 20 cm. Patients fasted for 6 h before PET; however, liberal water intake was encouraged.

A transmission scan was first obtained from the level of the upper neck to the pelvis, at 4 min per bed position. Immediately thereafter, the patient was injected with 370 MBq (10 mCi) ^{11}C-methionine. Acquisition of the emission scan was started 10 min later, at 6 min per bed position. All scans were reconstructed using vendor-provided filtered backprojection algorithms.

^{18}F-FDG PET

^{18}F-FDG was prepared using the PETtrace FDG MicroLab (General Electric Medical Systems). The ^{18}F-FDG PET scan was obtained a minimum of 2 h after completing the ^{11}C-methionine PET scan. Forty-five minutes after the injection of 370 MBq (10 mCi) ^{18}F-FDG, an emission scan was acquired from the neck to the pelvis, for 6 min per bed position.

Subsequently, a transmission scan was acquired for 4 min per bed position. This study was also reconstructed using vendor-provided filtered backprojection algorithms.

MRI

Modified MRI of the pelvis, including the retroperitoneum, was performed on a 1.5-T Signa MRI scanner (General Electric Medical Systems), using axial spin-echo T1- and T2-weighted images, with and without fat suppression. Selected patients also had MRI of the lower thoracic and lumbar spine, without gadolinium.

CT

Abdominal and pelvic CT scans were obtained on a high-speed CT/i helical scanner (General Electric Medical Systems). Contiguous 1-cm-thick tomographic slices were obtained after the intravenous bolus injection of nonionic contrast material.

Bone Scintigraphy and Bone Scan Index

Bone scans were done approximately 2 h after the intravenous injection of 925 MBq (25 mCi) ^{99m}Tc-methylene diphosphonate. Whole-body anterior and posterior images were acquired on a dual-head Genesys gamma camera (ADAC Laboratories, Milpitas, CA).

The bone scan index (BSI), a semiquantitative index that reflects the percentage of bony skeleton involved by the tumor, was also calculated. The BSI has been shown to have minimal interobserver and intraobserver variability and parallels the rise in the PSA level (*12*).

Data Analysis

The CT scans and MR images were read independently by a hospital radiologist. The bone scans were also read independently, with the BSI and the total number of lesions calculated for each patient.

The presence of bone metastasis was established on the basis of the bone scan findings of extensive characteristic lesions or, in cases with few abnormalities, on their subsequent progression on follow-up scans together with an increase in serum PSA level.

Lymph node metastasis was diagnosed on the basis of typical MRI or CT scan findings (or both) and was confirmed by interval progression over a 12-mo course. Lung metastasis and mediastinal metastasis were confirmed on the basis of persistent suspicious findings on follow-up chest x-rays, CT scans, and PET scans.

Transaxial, coronal, and sagittal PET images were evaluated visually by the same physician, who was unaware of the data from the other imaging modalities. The ^{11}C-methionine PET and ^{18}F-FDG PET scans were read independently. A PET scan was considered to be abnormal when a focus or an area of increased ^{18}F-FDG or ^{11}C-methionine uptake was above what is considered to be normal background. Regional ^{18}F-FDG and ^{11}C-methionine uptake in tumor tissue from the PET image data was quantified using standardized uptake values (SUVs). Each lesion was identified in the transaxial image, and SUV images were generated. Circular regions of interest were carefully drawn around each and every lesion on the ^{18}F-FDG PET and the ^{11}C-methionine PET images. The SUV values represent the maximal radioactivity concentration in the region of interest, normalized for injected dose and body weight.

Statistical Analysis

The sensitivity of each of the imaging modalities was calculated according to the number of lesions detected for each one of the studies compared with that of CIM (bone scan, CT scan, and MR image).

The SUV for each one of the lesions was determined on both PET scans. In addition, the mean, median, minimum, and maximum SUV for the bone and soft-tissue lesions was calculated for the ^{18}F-FDG PET and ^{11}C-methionine PET scans. The mean SUVs were compared by the paired *t* test. The difference between the proportion of lesions identified by ^{18}F-FDG PET and ^{11}C-methionine PET was compared using a McNemar test incorporating an adjustment method described by Eliasziw and Donner (*13*). Such an adjustment is necessary because the lesions on the same patient are likely to be correlated and one of the assumptions of the unadjusted McNemar test is violated. Statistical significance was determined from a $P < 0.05$.

Correlation between each pair of variables per patient, including the PSA, BSI, and number of lesions detected by each of the different imaging modalities, was examined by the Spearman rank correlation test.

Agreement between each pair of modalities was evaluated using the κ statistic, where $\kappa = 0$ when the agreement between the 2 modalities equals that expected by chance alone and $\kappa = 1$ when there is perfect agreement (*14*).

RESULTS

A total of 24 PET scans were obtained on 12 patients. Gleason scores of the primary prostate neoplasm ranged from 6 to 10. Table 1 presents details about the patients, including age, hormonal status, primary therapy given at the time of the scan, and PSA value upon entering the study.

The combination of CT, MRI, and bone scanning (CIM) detected a total of 348 of 348 lesions (100%), of which 325 of 348 (93%) were bone metastases and 23 of 348 (7%) were abdominal and pelvic soft-tissue lesions. CT and MRI of the chest were not part of the study, although a few patients had CT scans of the chest on follow-up visits. However, most of the lesions in metastatic prostate cancer will have been detected in our study by the combination of bone scanning plus CT and MRI of the abdomen and pelvis because the number of soft-tissue lesions above the diaphragm normally represents a small percentage, if any, of the total number of lesions.

PET scan findings were compared with the results of CIM. A total of 314 of 325 lesions (96.6%) were detected by bone scans on the 12 patients; however, 45 bone lesions were detected exclusively by PET, with 37 of them detected by ^{11}C-methionine PET. In 3 patients, 8 cervical spine metastases were detected only by PET. Nine additional suspicious bone lesions were detected only by MRI (in patients 2, 3, and 10). The number of bone metastases varied greatly between patients; some patients had multiple bone metastases (86 lesions), whereas others had none, entering the study on the basis of soft-tissue involvement (Fig. 1).

The BSI ranged from 0% to 69.9%. The bone scans of 2 of the patients with the highest values were cases of very extensive osseous metastases (superscan). The BSI had a highly significant correlation with the total number of suspicious lesions on the bone scan (0.876), which was slightly less correlated with the serum PSA value (0.859) (Table 2).

^{18}F-FDG PET detected a total 167 of 348 lesions (48.0%), including 157 of 325 bone lesions (48.3%), 7 of 23 abdom-

TABLE 1
Details of Patient's Age, PSA Value, BSI, Hormonal Status, and Treatment at Time of PET Scan

Patient no.	Age (y)	PSA (ng/mL)	BSI	Hormonal status	Treatment
1	77	231.6	10	Androgen dependent	Antiandrogen therapy
2	64	87	0	Androgen dependent	Vaccine protocol
3	69	14.9	0.9	Androgen dependent	Total androgen blockade
4	79	1,264.7	57.8	Androgen independent	Taxol-based regime
5	76	60.2	6.3	Androgen independent	Ketoconazole
6	69	3.4	2.0	Androgen independent	Taxol-based regime
7	66	48.7	1.4	Androgen independent	Lupron*
8	66	22.3	0	Androgen dependent	Antiandrogen therapy
9	73	24	4.7	Androgen dependent	Antiandrogen therapy
10	85	488	69.9	Androgen independent	Prednisone
11	46	35	0	Androgen independent	No specific treatment at time of scan
12	69	191	21.1	Androgen independent	Antiandrogen withdrawal

*Lupron (leuprolide acetate; TAP Pharmaceuticals, Lake Forest, IL).

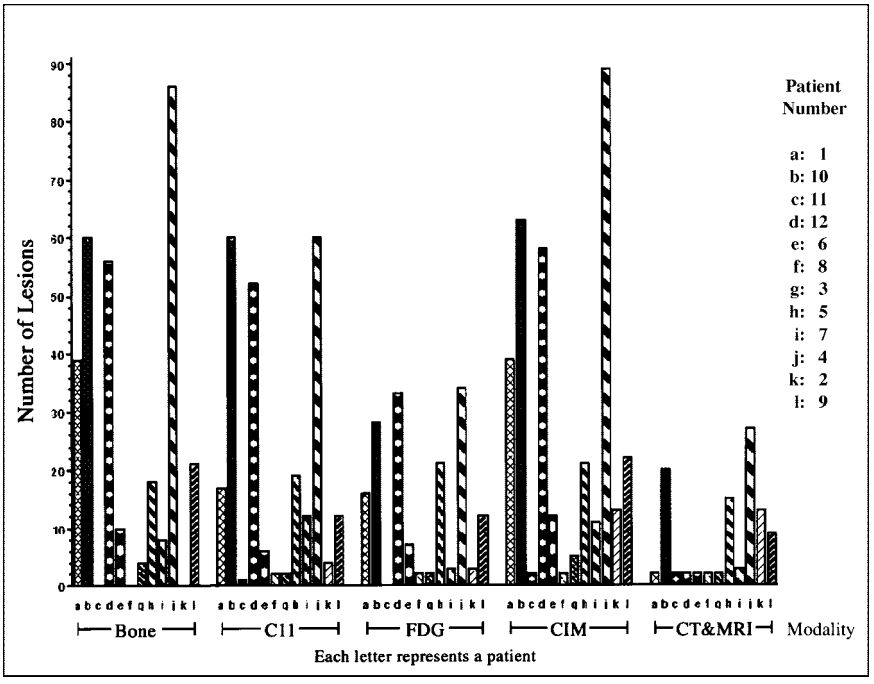

FIGURE 1. Histogram shows number of lesions detected in each patient by different imaging modalities. Bone = bone scintigraphy; C11 = ^{11}C-methionine PET; FDG = ^{18}F-FDG PET.

inal or pelvic lesions (30.4%), and 3 chest or neck soft-tissue lesions. In general, when the patient had a prominent tumor burden, osseous metastases were detected readily by ^{18}F-FDG PET. The SUV of bone lesions ranged from 1.2 to 7.7, with 3.4 as the mean and 3.1 as the median. For soft-tissue lesions, the SUV ranged from 2.2 to 7.9, with 4.1 as the mean and 3.6 as the median (Table 3).

^{11}C-Methionine PET scanning detected a total of 251 of 348 lesions (72.1%), with 227 of 325 bone metastases (69.8%), 16 of 23 abdominal and pelvic soft-tissue lesions (69.6%), and 8 neck and chest soft-tissue lesions. In the cases of the superscan, the number of bone metastases detected by ^{11}C-methionine PET correlated much better than ^{18}F-FDG PET with the number of lesions seen on the bone scan. In general, lesions detected by ^{18}F-FDG PET were also detected by ^{11}C-methionine PET; conversely, ^{11}C-methionine PET detected many more additional lesions than ^{18}F-FDG PET. However, in 2 patients, ^{18}F-FDG PET detected 5 bone and 2 soft-tissue lesions not detected by ^{11}C-methionine PET. The SUV of bone lesions ranged from 13.1 to 1.5, with 4.8 as the mean and 4.7 as the median. For soft-tissue lesions, the SUV ranged from 8.9 to 2.8, with 5.1 as the mean and 4.9 as the median. The difference in means was found to be statistically significant ($P < 0.01$) with a paired t test. Hence, we conclude that the mean uptake of ^{11}C-methionine was higher than the mean uptake of ^{18}F-FDG.

The difference in the proportion of lesions detected was also found to be statistically significant ($P < 0.01$) using an adjusted McNemar test (*13*). On the basis of this study, the sensitivity for the detection of bone and soft-tissue metastases with ^{18}F-FDG PET was 48.3% and 30.4%, respectively; whereas for ^{11}C-methionine PET it was considerably better, 69.8% and 69.6%, respectively. Table 4 summarizes the results of the study.

DISCUSSION

Over the years, ^{18}F-FDG PET has proven to be a formidable imaging technique for a great variety of malignant tumors (*15*). Since the initial descriptions by Di Chiro et al. (*16*) of increased ^{18}F-FDG uptake in brain neoplasms, there

TABLE 2
Spearman Rank Correlation per Patient Between PSA, BSI, and Different Imaging Modalities

	PSA	BSI	Bone	CT and MRI	^{18}F-FDG PET	^{11}C-Methionine PET	CIM
PSA	1.000	0.822	0.859	0.785	0.703	0.773	0.874
BSI		1.000	0.876	0.761	0.790	0.916	0.884
Bone			1.000	0.637	0.937	0.950	0.993
CT and MRI				1.000	0.612	0.651	0.686
^{18}F-FDG PET					1.000	0.942	0.934
^{11}C-Methionine PET						1.000	0.955

TABLE 3
SUVs for Bone and Soft-Tissue Lesions on ^{11}C-Methionine PET and ^{18}F-FDG PET

	^{18}F-FDG PET		^{11}C-Methionine PET	
Parameter	Bone	Soft tissue	Bone	Soft tissue
Mean	3.4	4.1	4.8	5.1
Median	3.1	3.6	4.7	4.9
Max. SUV	7.7	7.9	13.1	8.9
Min. SUV	1.2	2.2	1.5	2.8

Max. = maximum; Min. = minimum.

has been continuous interest and research in the applications of ^{18}F-FDG PET in oncology. Nevertheless, its application in such an important neoplasm as prostate cancer has not met the expectations. One of the main reasons has been the limited sensitivities of ^{18}F-FDG PET in metastatic prostate cancer, ranging from as low as 18% in a study done by Yeh et al. (*17*) to 65% in a study done by Shreve et al. (*18*). Using ^{11}C-methionine PET, Nilsson et al. (*19*) found methionine uptake in a considerable number of lesions in patients with androgen-resistant prostate cancer. Inoue et al. (*11*) compared ^{18}F-FDG PET with ^{11}C-methionine PET in a variety of tumors, which did not include prostate cancer, and imaged only a limited part of the patient's body; however, the sensitivities were 64.5% and 61.3% for ^{18}F-FDG PET and ^{11}C-methionine PET, respectively. More recently, we have shown that a high proportion of clinically active index lesions are metabolically active, with sensitivities of 85% and 95% for ^{18}F-FDG PET and ^{11}C-methionine PET, respectively (*20*). However, this study analyzed only index lesions (index lesions being the clinically active lesions that were detected by conventional imaging studies, which could be positive on a PET scan, representing a finding for future follow-up studies).

Evaluation of the extent of disease in prostate cancer, especially when there is biochemical or clinical evidence of disease progression, is of vital importance. Traditionally, this evaluation has been done with serial bone and CT scans and more recently with MR images. Nevertheless, these imaging techniques, though very precise anatomically (especially MRI), are limited in the extent of the body imaged and in their ability to distinguish benign from malignant tissue. Even with serial bone scans, it is frequently difficult to evaluate treatment response because the scan appearances may falsely indicate progression attributed to a flare-up response of the bone in the process of repairing or healing from the injury of the tumor. Moreover, sclerotic non–tumor-bearing lesions tend to appear on bone scans as suspicious findings for long periods of time.

The serum tumor marker PSA has represented a great advance in the management of the patient with prostate cancer. However, it is limited in its ability to evaluate and quantify or semiquantify the tumor burden. In addition, sometimes tumor progression may not be accompanied by a parallel rise in PSA because of, for example, tumor dedifferentiation (*21*). Thus, there is an obvious need for a metabolic imaging modality such as PET, which reflects the differences in the metabolism of tumor cells in comparison with normal tissue.

Our study shows, as reported by Macapinlac et al. (*22*), that whole-body ^{11}C-methionine PET is a feasible technique that can produce high-quality images, despite the short physical half-life of ^{11}C-methionine (Fig. 2). We have been able to routinely perform ^{11}C-methionine PET and ^{18}F-FDG PET scanning on the same day separated by a 3- or 4-h period.

The sensitivity of 72.1% (251/348 lesions) obtained in our study for the detection of bone and soft-tissue metastases with ^{11}C-methionine PET is fairly high, at least in comparison with previously reported values with ^{18}F-FDG PET of 18%–65% (*17*,*18*). However, the sensitivity of 48% (167/348 lesions) for ^{18}F-FDG PET in our study (for bone and soft-tissue metastasis) is more in concordance with these earlier results. The ability of ^{11}C-methionine PET to detect more bone and soft-tissue metastases than ^{18}F-FDG PET is not surprising (Fig. 3) if we consider that prostate cancer can be a heterogeneous tumor with a wide spectrum in biologic behavior, ranging from indolent tumors to more aggressive ones, often in younger men, which can kill the patient in a few years. Therefore, the difference in uptake of the 2 tracers probably reflects the diversity and differences in tumor metabolism, not only from patient to patient but also frequently in the same patient between metastases. Still, a significant proportion of lesions (26%) had no detectable metabolism of ^{18}F-FDG or ^{11}C-methionine. Although technical factors cannot be totally excluded, we believe that metabolically inactive sites may be necrotic or dormant. Thus, bone scans can overestimate the extent of disease. Conversely, a few bone lesions were detected

TABLE 4
Number and Percentage of Lesions Detected with Each Imaging Modality in 12 Patients Included in Study

	Number (percentage) of lesions			
		Soft tissue		
Imaging modality	Bone	Neck and chest	Abdomen and pelvis	Total
^{18}F-FDG PET	157 (48.3)	3	7 (30.4)	167 (48)
^{11}C-Methionine PET	227 (69.8)	8	16 (69.6)	251 (72.1)
Bone scan	314 (96.6)	0	0	314 (90.2)
CT and MRI	78 (24)	*	23 (100)	101 (29)
CIM†	325 (100)	0	23 (100)	348 (100)

*Not imaged.
†CT, MRI, and bone scan.

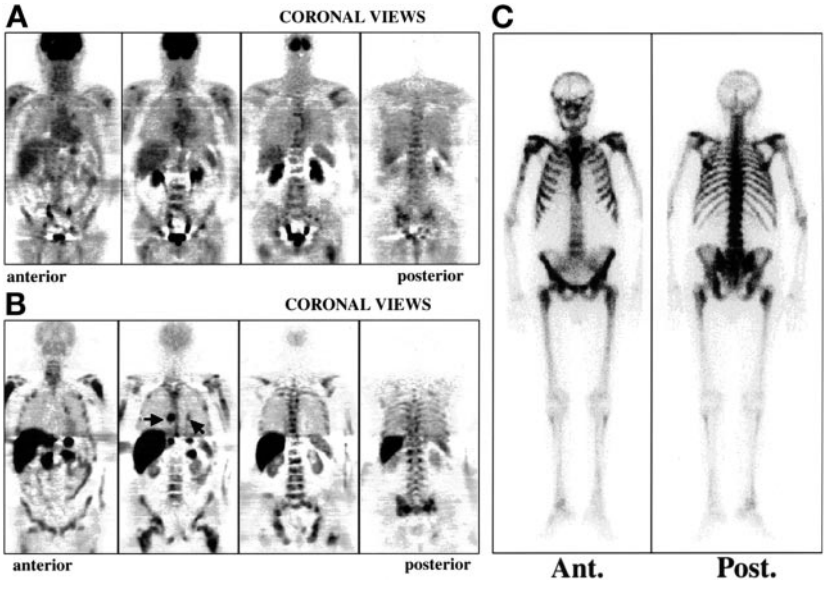

FIGURE 2. Different biodistributions of ^{18}F-FDG (A) and ^{11}C-methionine (B) in PET studies of patient 10. More lesions were detected with ^{11}C-methionine PET (B) than with ^{18}F-FDG PET (A). Arrows point to soft-tissue lesions detected only by ^{11}C-methionine PET. (C) Anterior (Ant.) and posterior (Post.) whole-body images of corresponding bone scan (superscan).

earlier by PET rather than by bone scanning, which reflects the ability of PET to detect the initial tumor cluster located in the bone marrow before it can be seen on the bone scan (Fig. 3).

The difference in lesion detection between ^{11}C-methionine and ^{18}F-FDG (69.6% and 30.4%, respectively) is even more pronounced if we consider soft-tissue metastases in the abdomen and pelvis. This difference may be attributed to several causes: (a) Minimal activity of ^{11}C-methionine was found in the bladder in comparison with ^{18}F-FDG, with the latter interfering with the evaluation of pelvic structures. Even with new reconstruction algorithms, ^{11}C-methionine is clearly superior for the evaluation of metastases in the pelvis. (b) In comparison with ^{11}C-methionine, which has minimal excretion through the kidneys, the higher concentration of ^{18}F-FDG in the collecting system, pelvis, and ureter of both kidneys diminishes the ability to detect ab-

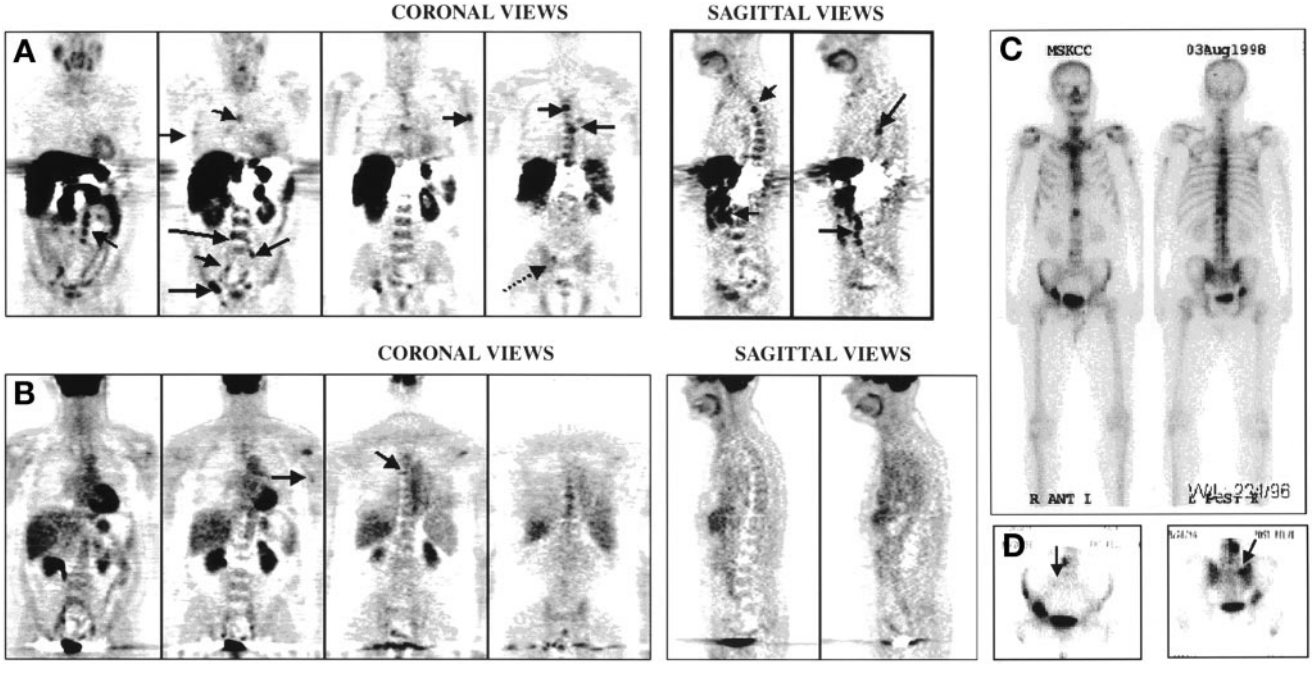

FIGURE 3. Coronal and sagittal views of ^{11}C-methionine PET (A) and ^{18}F-FDG PET (B) studies of patient 7. Many more lesions (arrows), including lesions in soft tissues, are detected by ^{11}C-methionine PET (A) than by ^{18}F-FDG PET (B). Because of low excretion of ^{11}C-methionine by kidney, abdominal and pelvic lymphadenopathy was better detected by ^{11}C-methionine PET than by ^{18}F-FDG PET (arrows in abdomen and pelvis). Lesion in right sacroiliac joint detected by ^{11}C-methionine PET (arrow with broken shaft) was not evident on bone scan (C) or on ^{18}F-FDG PET scan. ANT = anterior; POST = posterior. (D) Arrows point to lesion in anterior and posterior spot views of pelvis on bone scan obtained 2 mo later.

dominal retroperitoneal metastases. (c) Inherent metabolic differences of tumor cells favoring preferential uptake and metabolism of ^{11}C-methionine over ^{18}F-FDG may in part play a role. This might explain the differences observed in the SUVs of bone and soft-tissue metastases, where ^{11}C-methionine PET has consistently higher values in both types of tissues.

We found that cervical spine metastases were more easily detected by PET than by bone scintigraphy. In 3 patients, a total of 8 cervical spine metastases not detected by bone scintigraphy were clearly evident on the ^{18}F-FDG PET and ^{11}C-methionine PET scans (Fig. 4). The study by Schirrmeister et al. (*23*) confirms this finding; they found that the sensitivity of bone scintigraphy in comparison with ^{18}F PET was only 20% in the cervical spine. Conversely, rib metastases were the most difficult metastases to detect with PET, not only because the SUV in ^{18}F-FDG PET was as low as 1.2 for some metastases but also because the small cross-sectional area of the ribs limited the ability to detect the metastasis, even with a dedicated PET scanner—especially if the lesions were not very prominent. The use of a rotating 3-dimensional display helps in the detection of metastases in the rib cage. In general, the SUVs were higher than 1.2. ^{11}C-Methionine PET had consistently higher SUVs than ^{18}F-FDG PET in both bone and soft-tissue lesions (Table 3), and the difference in means was statistically significant between these 2 modalities ($P < 0.01$). Similarly, a statistically significant difference was found between the proportions of lesions found by ^{11}C-methionine PET and ^{18}F-FDG PET ($P < 0.01$). Conversely, the mean SUVs between bone and soft-tissue lesions did not differ significantly for ^{18}F-FDG PET ($P = 0.25$) and for ^{11}C-methionine PET ($P = 0.36$).

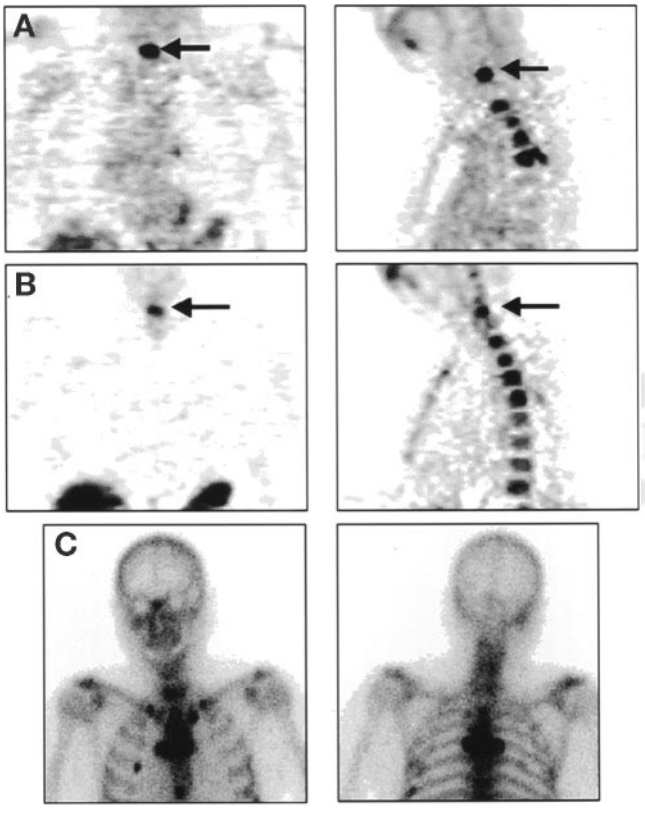

FIGURE 4. Representative ^{18}F-FDG PET (A), ^{11}C-methionine PET (B), and bone scintigraphy (C) images of neck and upper chest of patient 5. Arrows point to bone metastasis in lower cervical spine easily seen on PET images but not clearly evident on bone scan.

Another question of interest for us was the correlation of PSA and BSI with the total number of lesions detected by each modality. The Spearman rank correlation was calculated between each pair of modalities or variables (Table 2). CT and MRI had the lowest correlation with the other modalities. Of all 21 possible pairwise correlations, the 6 that involved CT and MRI were the lowest, the highest of these being the one with PSA (0.785). ^{11}C-Methionine PET and BSI had a higher correlation (0.916) than that for bone scan and BSI (0.876), whereas ^{18}F-FDG PET and BSI had a lower correlation of 0.790. Both PET modalities correlated well with bone scanning (0.937 for ^{18}F-FDG and 0.950 for ^{11}C-methionine) and CIM (0.934 for ^{18}F-FDG and 0.955 for ^{11}C-methionine). Evaluation of the agreement between each pair of variables (κ statistic) shows that bone scan and CIM agree very well (0.930), which is not surprising because the bone scan is part of CIM and identifies most of the lesions. The agreement between ^{11}C-methionine PET and CIM (0.539) is higher than that between ^{18}F-FDG PET and CIM (0.431). The differences between ^{18}F-FDG PET and ^{11}C-methionine PET, in comparison with CIM, are more pronounced than the rank correlations reported above (Table 5).

One of the advantages of the PET scan is that it can provide an indication of the metabolic activity of the disease in a single study and anatomically localize metastatic sites in bone and soft tissues. As such, PET could be an extremely useful adjunct to refine increasingly accurate nomograms used to estimate the pre- and postsurgical likelihood of nodal and distant metastases in prostate cancer (*24–26*).

In ongoing clinical studies using ^{11}C-methionine PET and ^{18}F-FDG PET in prostate cancer patients, we have found that these PET studies can assess the response to treatment as early as 4 wk after starting or changing treatment, with improvement or worsening of the PET scan findings, in many cases with no significant changes on the bone scans. Similar to what was seen in a study by Agus et al. (*27*) using male mice with the CWR22 human prostate cancer xenograft model, the changes observed on the ^{18}F-FDG PET scan have paralleled the changes seen in serum PSA (Fig. 5). Therefore, the main value of PET for the prostate cancer patient may be to evaluate changes in tumor burden and location of disease, using this information to monitor the effect of treatment and determine the prognosis of the patient. We have also found that ^{18}F-FDG PET can detect native, residual, or recurrent disease in the prostate bed,

TABLE 5
Agreement Between Different Imaging Modalities Using κ Statistics

	Bone	CT and MRI	^{18}F-FDG PET	^{11}C-Methionine PET	CIM
Bone	1.000	0.244	0.435	0.526	0.930
CT and MRI		1.000	0.338	0.291	0.392
^{18}F-FDG PET			1.000	0.617	0.431
^{11}C-Methionine PET				1.000	0.539
CIM					1.000

largely because of iterative reconstruction algorithms that allow a better visualization of the anatomic structures adjacent to the bladder, including the prostate bed (Fig. 6).

This study had certain limitations. Our study, like others, was limited by the inability to prove with certainty the metastatic nature of all lesions detected with PET, because pathologic confirmation of all PET findings is impractical and unethical. In addition, there was a lack of CT and MRI studies of the chest to correlate the PET scan findings in the chest. The PET scans were obtained from the neck to the pelvis; therefore, bone scan findings in the lower extremities and skull (17 lesions in our study) could not be correlated.

The PET scanner itself has the known limitation of not being able to detect microscopic disease. Artifacts from the attenuation correction with filtered backprojection reconstruction techniques were present around areas of high activity concentration, such as the liver with ^{11}C-methionine PET and the bladder and kidneys with ^{18}F-FDG PET. In addition, skull metastases are not detected with ^{18}F-FDG PET because of the high activity concentration in the brain. We have found that the intrinsically higher activities seen in the bone marrow with ^{11}C-methionine PET in comparison with ^{18}F-FDG PET does not limit the ability to differentiate a bone metastasis from normal bone tissue (Fig. 4).

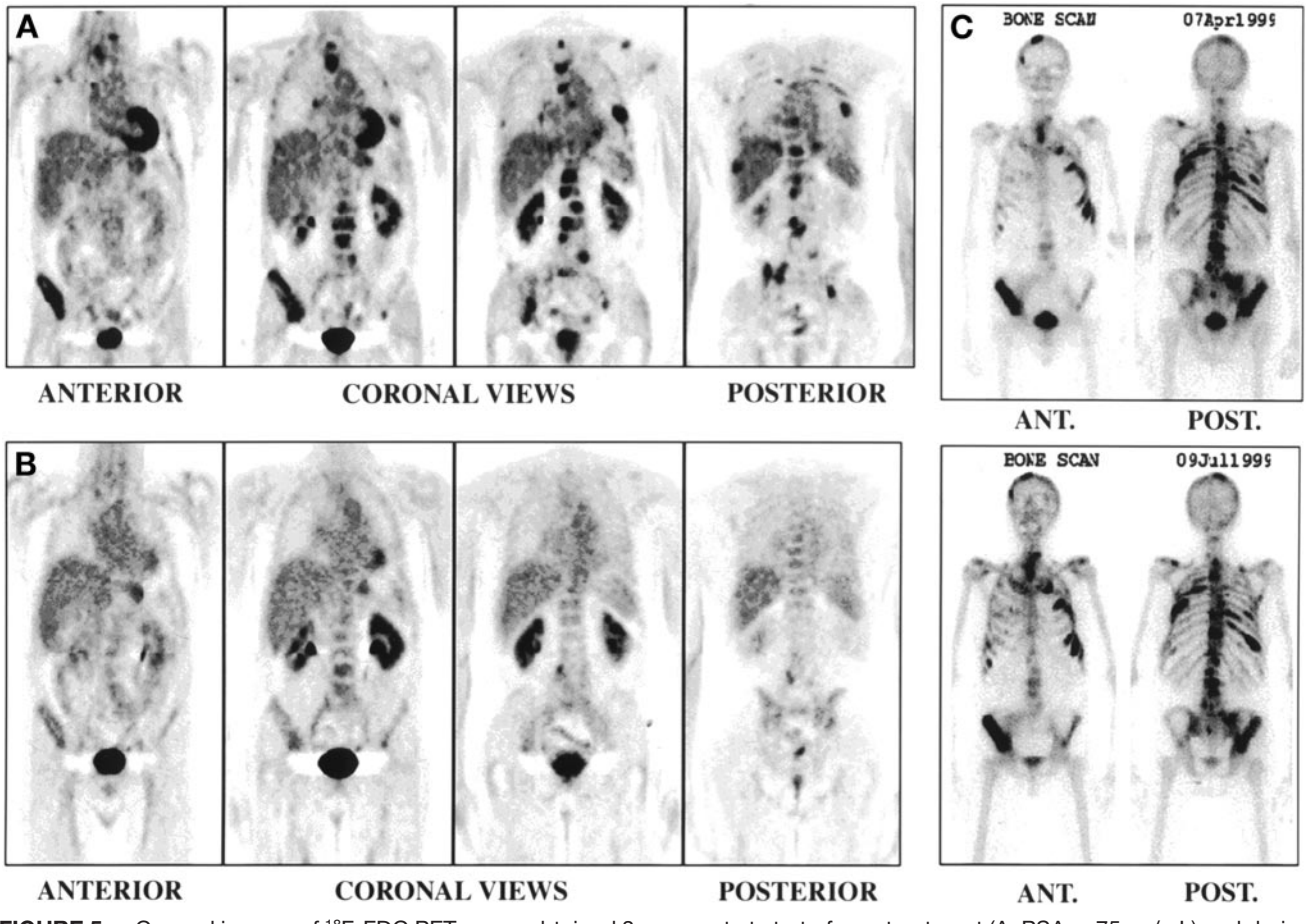

FIGURE 5. Coronal images of ^{18}F-FDG PET scans obtained 3 mo apart at start of new treatment (A; PSA = 75 ng/mL) and during follow-up (B; PSA = 8.6 ng/mL). Note significant improvement with parallel decrease in PSA, whereas basically no change is seen on corresponding bone scans (C) obtained on same day as ^{18}F-FDG PET scans. ANT. = anterior; POST. = posterior.

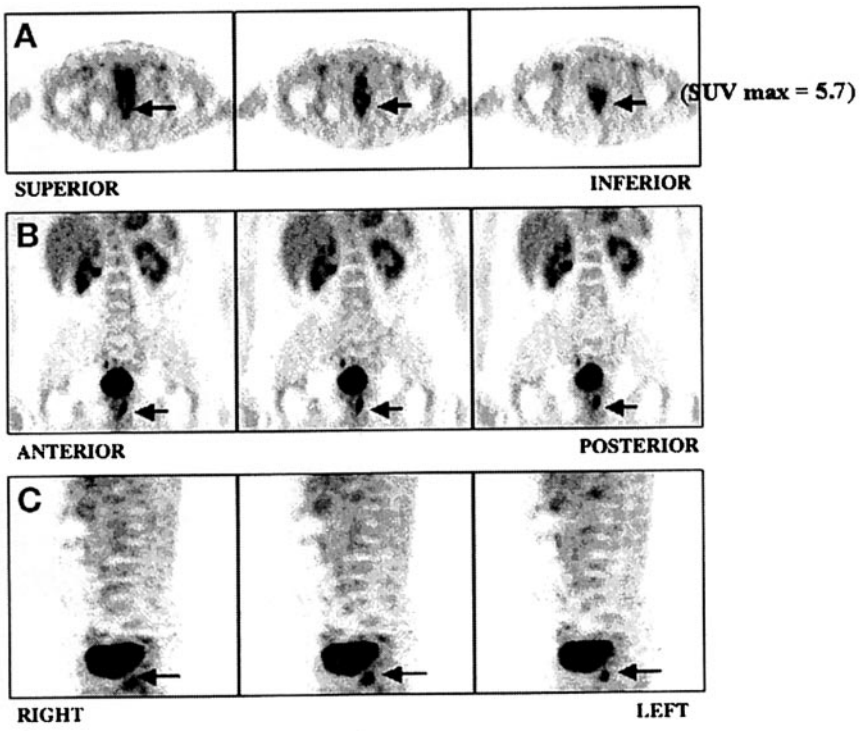

FIGURE 6. ^{18}F-FDG PET transaxial (A), coronal (B), and sagittal (C) views (ordered-subsets expectation maximization/segmented attenuation-corrected reconstruction was performed) of abdomen and pelvis of 70-y-old man with prostate cancer and rising PSA level (16.8 ng/mL). Patient was initially treated 5 y before study with radical prostatectomy followed by radiation therapy to prostate bed. Arrows point to recurrent tumor in prostate bed region, which was later confirmed by biopsy.

CONCLUSION

Whole-body ^{11}C-methionine PET is a feasible imaging technique that detects significantly more bone and soft-tissue lesions than ^{18}F-FDG PET, allowing the assessment of tumor metabolism in the frequently biologically heterogeneous metastases of prostate cancer patients. Two possible explanations for the differences are as follows: (a) differences in tumor metabolism between patients and in the same patient between metastases, and (b) a time-dependent metabolic cascade in advanced prostate cancer, with initial uptake of ^{11}C-methionine in dormant sites followed by increased uptake of ^{18}F-FDG during progression of the disease. Therefore, ^{11}C-methionine PET is a potentially valuable imaging technique for the assessment and monitoring of tumor response to treatment, an area in which CIM, including bone scans (despite having increased sensitivity), have well-known limitations.

ACKNOWLEDGMENTS

The authors thank Ronald Finn, PhD, for preparation and quality assurance of the radiotracers; Richard Petrisco for data management; Dr. Samuel Yeh for helpful commentaries and reviewing the manuscript; and Dr. Roland Chisin for many helpful insights, suggestions, and reviewing the manuscript. This study was supported by grants from the Hascoe Foundation and National Institutes of Health/National Cancer Institute grant 1P50 CA86438 01.

REFERENCES

1. Garnick MB, Fair WR. Prostate cancer. *Sci Am*. 1998;279:74–83.
2. Mettlin C, Jones GW, Murphy GP. Trends in prostate cancer in the United States, 1974–1990: observations from the patient care evaluation studies of the American College of Surgeons Commission on Cancer. *CA Cancer J Clin*. 1993;43: 83–91.
3. Sher HI, Chung WK. Bone metastases: improving the therapeutic index. *Semin Oncol*. 1994;21:630–656.
4. Sagalowsky AI, Wilson JD. Hyperplasia and carcinoma of the prostate. In: Fauci AS, Braunwald E, Iselbacher K, Wilson D, eds. *Harrison's Principles of Internal Medicine*. 14th ed. New York, NY: McGraw-Hill; 1998:596–602.
5. Castelino RA, DeLa Paz RL, Larson SM. Imaging techniques in cancer. In: DeVita VT, Hellman S, Rosenberg SA, eds. *Cancer: Principles and Practice of Oncology*. 4th ed. Philadelphia, PA: Lippincott-Raven; 1993.
6. Fisher G, Ruschenburg I, Eigenbrodt E, Katz N. Decrease in glucokinase and glucose-6-phosphatase and increase in hexokinase in putative preneoplastic lesions of the rat liver. *J Cancer Res Clin Oncol*. 1987;113:430–436.
7. Ishiwata W, Ido T, Vaalburg W. Increased amount of D-enantiomer dependent on alkaline concentration in the synthesis of L-[1-^{11}C]methionine. *Appl Radiat Isot*. 1988;39:311–314.
8. Miyazawa H, Arai T, Lio M, Hara T. PET imaging of non-small-cell lung carcinoma with carbon-11-methionine: relationship between radioactivity uptake and flow cytometric parameters. *J Nucl Med*. 1993;34:1886–1891.
9. Lindholm P, Leskinen-Kallio S, Minn H, et al. Comparison of fluorine-18-fluorodeoxyglucose and carbon-11-methionine in head and neck cancer. *J Nucl Med*. 1993;34:1711–1716.
10. Leskinen-Kallio S, Ruotsalainen U, Någren K, Teräs M, Joensuu H. Uptake of carbon-11-methionine and fluorodeoxyglucose in non-Hodgkin's lymphoma: a PET study. *J Nucl Med*. 1991;32:1211–1218.
11. Inoue T, Kim EE, Wong FC, et al. Comparison of fluorine-18-fluorodeoxyglucose and carbon-11-methionine PET in detection of malignant tumors. *J Nucl Med*. 1996;37:1472–1476.
12. Imbriaco M, Larson SM, Yeung HW, et al. A new parameter for measuring metastatic bone involvement by prostate cancer: the bone scan index. *Clin Cancer Res*. 1998;4:1765–1772.
13. Eliasziw M, Donner A. Application of the McNemar test to non-independent matched pair data. *Stat Med*. 1991;10:1981–1991.

14. Cohen J. The measurement of interrater agreement. In: Fleiss JL, ed. *Statistical Methods for Rates and Proportions*. New York, NY: Wiley; 1981:212–236.
15. Strauss LG, Conti PS. The applications of PET in clinical oncology. *J Nucl Med*. 1991;32:623–648.
16. Di Chiro G, DeLaPaz RL, Brooks RA, et al. Glucose utilization of cerebral gliomas measured by [^{18}F]fluorodeoxyglucose and positron emission tomography. *Neurology*. 1982;32:1323–1329.
17. Yeh S, Imbriaco M, Larson S, et al. Detection of bony metastases of androgen independent prostate cancer by FDG-PET. *Nucl Med Biol*. 1996;23:693–697.
18. Shreve PD, Grossman HB, Gross MD, Wahl RL. Metastatic prostate cancer: initial findings of PET with 2-deoxy-2-[F-18]fluoro-D-glucose. *Radiology*. 1996; 199:751–756.
19. Nilsson S, Kalner K, Ginman C, et al. C-11 methionine positron emission tomography in the management of prostatic carcinoma. *Antibody Immunoconj Radiopharm*. 1995;8:23–38.
20. Osman I, Akhurst T, Macapinlac H, et al. C-11 methionine and F-18 PET imaging: use in the evaluation of progressive prostate cancer [abstract]. *Proc Am Soc Clin Oncol*. 1998;17:312-A.
21. Eisenberger MA, Nelson WG. How much can we rely on the level of prostate-specific antigen as an end point for evaluation of clinical trials? A word of caution! *J Natl Cancer Inst*. 1996;88:779–781.
22. Macapinlac HA, Humm JL, Akhurst T, et al. Differential metabolism and pharmacokinetics of L-[1-^{11}C]-methionine and 2-[^{18}F]fluoro-2-deoxyglucose (FDG) in androgen independent prostate cancer. *Clin Positron Imaging*. 1999;2: 173–181.
23. Schirrmeister H, Guhlmann A, Elsner K, et al. Sensitivity in detecting osseous lesions depends on anatomic localization: planar bone scintigraphy versus ^{18}F PET. *J Nucl Med*. 1999;40:1623–1629.
24. Kattan MW, Stapleton AM, Wheeler TM, Scardino PT. Evaluation of a nomogram used to predict the pathologic stage of clinically localized prostate carcinoma. *Cancer*. 1997;79:528–537.
25. Kattan MW, Eastham JA, Stapleton AM, Wheeler TM, Scardino PT. A preoperative nomogram for disease recurrence following radical prostatectomy for prostate cancer. *J Natl Cancer Inst*. 1998;90:766–771.
26. Kattan MW, Wheeler TM, Scardino PT. Postoperative nomogram for disease recurrence after radical prostatectomy for prostate cancer. *J Clin Oncol*. 1999; 17:1499–1507.
27. Agus DB, Golde DW, Sgouros G, Ballangrudm A, Cordon-Cardo C, Sher IH. Positron emission tomography of a human prostate cancer xenograft: association of changes in deoxyglucose accumulation with other measures of outcome following androgen withdrawal. *Cancer Res*. 1998;58:3009–3014.